Regulation of Substrate Dissipation via Tunable Linear Elasticity Controls Cell Activity

Pasquale Sacco, Francesco Piazza, Chiara Pizzolitto, Gabriele Baj, Francesco Brun, Eleonora Marsich, and Ivan Donati*

Natural tissues and extracellular matrices (ECMs) are not purely elastic materials but exhibit dissipative properties. Although it has recently emerged as a novel regulator of cellular responses, the contribution of material dissipation to guiding cell-fate decisions is still in its infancy. Here, a strategy for tuning the dissipation rate of viscoplastic substrates while precisely regulating linear elasticity is reported. Semi-interpenetrating substrates consisting of a rigid hydrogel network intertwined with a branched biopolymer are described. The release of these weak physical entanglements under loading dissipates the applied stress and leads to the extension of the linear elasticity. These results reveal a crucial link between this material property and cell response in 2D cultures, impacting cell migration mode and speed, vinculin-dependent focal adhesion geometry and size, F-actin organization, the transmission of forces, and Yes-associated protein nuclear translocation. It is shown that cells require joint actomyosin contractility and microtubule tension to probe the substrate and decide whether or not to adhere, revealing a clear correlation between force transmission, substrate dissipation rate, and amount of anchoring points. Overall, these findings introduce linear elasticity as a novel design parameter for assembling tunable dissipative materials to study cell mechanosensing in 2D and possibly also in 3D cultures.

1. Introduction

Extracellular matrices (ECMs), and more broadly native tissues, exhibit complex mechanical behaviors including viscoelasticity, plasticity, and nonlinear elasticity. Rather than being purely elastic, biological milieus manifest a time- and frequency-dependent response to loading or deformation, with dissipation of forces exerted to deform them.[1] Mechanistically, ECMs can dissipate forces under loading depending on the nature of cross-links,[2,3] both slipping and sliding phenomena,[4,5] the release of polymer entanglements, protein unfolding, and poroelastic effects.[1] Under 2D conditions, cells probe the underlying substrate rigidity through the molecular clutch machinery, that is myosin-actin-integrin axis.[6–8] Upon tethering to ECM proteins, cells generate and transmit forces outward, eliciting intracellular mechanotransduction processes entailing talin unfolding and ensuing vinculin binding,[9] focal adhesion assembly,[10] alteration of lamin A expression,[11] and nuclear translocation of the Yes-associated protein (YAP).[12] Given the emerging role of force dissipation linked to ECM in cell mechanobiology,[1,13] the molecular clutch model has been generalized introducing dissipative contributions,[14,15] revealing that viscosity can suppress reduced stiffness in modulating cell functions if substrate stress relaxation is set in between the timescale for clutch binding (≈1 s) and its characteristic lifetime (≈10 to 100 s neglecting clutch reinforcement). Over the last few years, intriguing strategies aimed at developing bioengineered materials recapitulating ECM mechanics and timescales have been undertaken. Dissipative viscoelastic materials composed of polyacrylamide,[16–18] alginate,[19,20] chitosan,[21] and poly(ethylene glycol)[22,23] are gradually replacing unnatural, purely elastic substrates as models to understand and eventually predict functional responses of cells in terms of morphology, proliferation, and differentiation. Engineering the network architecture through the combination of different molecular weights or the coupling of spacers to the constituent polymers, as well as modulating the total number, affinity and ratio of weak/covalent bonds yield attractive approaches to tune the viscoelasticity of materials independent of the initial elastic modulus.[24–31] Here, we present a smart approach to alter substrate dissipation while precisely regulating linear elasticity. By incorporating a varying amount of weak physical entanglements into a rigid polymer network, we provide evidence to extend the linear stress–strain

P. Sacco, F. Piazza, G. Baj, I. Donati
Department of Life Sciences
University of Trieste
Via Licio Giorgieri 5, Trieste I-34127, Italy
E-mail: psacco@units.it
P. Sacco
AREA Science Park
loc. Padriciano 99, Trieste I-34149, Italy
P. Sacco, C. Pizzolitto, E. Marsich
Department of Medicine
Surgery and Health Sciences
University of Trieste
Piazza dell'Ospitale 1, Trieste I-34129, Italy
F. Brun
Department of Engineering and Architecture
University of Trieste
Via A. Valerio 6/1, Trieste I-34127, Italy

regime, as the release of entanglements dissipates the applied load and delays the fracture of the material. Furthermore, we demonstrate that this material property results a pivotal trait instructing cells whether and how to anchor the substrate in 2D cultures. This impacts key aspects such as cell adhesion growth, migration mode, cytoskeletal organization, transmission of forces, and transduction of biophysical cues.

2. Results

2.1. Substrates with Tunable Linear Elasticity

First, we aimed at developing a set of materials with adaptable linear elasticity, similar initial elastic modulus and fast stress relaxation. To achieve this goal, semi-interpenetrating polymer networks composed of agarose incorporating different amounts of uncrosslinked lactose-modified chitosan (CTL) were assembled using a 3-step procedure: i) preparation of CTL solutions in phosphate buffer; ii) addition of agarose powder; iii) temperature-assisted gelation (Experimental Section; Appendix S1, Supporting Information). CTL was selected as the unbound polymer because of its chain semi-flexibility, low viscosity, optimal solubility, and nearly uncharged nature at neutral pH.[32,33] We hypothesized that we can leverage the architecture of agarose networks to keep the initial elastic modulus of substrates constant and achieve fast stress relaxation while significantly modulating linear elasticity by adding CTL.

This is confirmed by the extension of the critical strain marking the onset of nonlinear region up to ≈3% (**Figure 1**a,b; Appendix S2, Supporting Information), the time needed to relax the stress to half of the initial value, $\tau_{0.5}$, in the range of 10–80 s (Figure S1, Supporting Information) and the calculation of the elastic modulus (≈19 kPa) for substrates with different compositions (Figure 1c). The loss tangents at 0.1 Hz[18] derived from the mechanical spectra (Figure S2, Supporting Information) do not vary significantly (Figure 1d), indicating similar viscoelasticity for substrates with different CTL content. In addition, substrates exhibit permanent deformation (plastic behavior) in the range of 15–30% (Figure S3, Supporting Information). 3D renderings of the internal network architecture obtained by confocal microscopy show optimal homogeneity, with CTL well dispersed throughout agarose matrix without forming polymer aggregate domains (Figure 1e). Of note, swelling and degradation studies demonstrate the structural stability of substrates with different compositions over a 7-day period after incubation under cell culture conditions (Figure S5, Supporting Information). Collectively, these findings reveal a controlled approach to assemble viscoplastic substrates with tunable linear elasticity but similar initial elastic modulus, fast stress relaxation, without significant swelling, or degradation.

To elucidate the mechanism underlying the difference in linear elasticity, creep experiments were performed under uniaxial compression conditions and the agarose mass, indicating polymer flow under loading, was calculated by ^{1}H-NMR spectroscopy (Figure 1f). The progressive decrease in matrix flux as well as agarose content in the lower part of the hydrogels clearly indicate that the resistance of the network to slippage increases with increasing amount of CTL. Therefore, this approach is predicted to increase the applied load to release the weak entanglements between the polymer chains and thus extend the linear elasticity (Figure 1g).

2.2. Cell anchorage is Governed by Substrate Dissipation and Requires Joint Actomyosin Contractility and Microtubule Tension

Next, we calculated the extent of dissipation linked to the release of weak entanglements for substrates with different compositions (**Figure 2**a,b; Appendix S4, Supporting Information).[21] Agarose does not provide integrin binding sites for cell anchorage, hence protein motifs can be covalently coupled to the polymer to enhance substrate–cell interactions.[34,35] Here, we exploited the presence of serum in the cell culture medium to form a protein coating on the substrates to avoid chemical functionalization of agarose. This approach ensures the adsorption of a comparable amount of proteins regardless of substrate type (Figure 2c). The efficacy of serum coating in promoting cell adhesion was tested in a control experiment (Figure S7, Supporting Information). When MG63 cells are seeded on substrates with different dissipation but similar elastic modulus (≈19 kPa) a progressive decrease in both cell number per surface area and cell spreading is observed (Figure 2d–g). Interestingly, cells spread similarly atop non-dissipative substrates and plastic wells (Figure 2g). Remarkably, a correlation is identified between cell spread and the number of cells per substrate area (Figure 2h), suggesting the compelling hypothesis that both processes are controlled by the same biological machinery.

Beside dissipation associated with the substrate itself, cells can dissipate forces through the dynamic remodeling of cell-extracellular matrix binding sites, intracellular damping due to creep or viscous slippage between the cytoplasm and the stress fibers, and the interfacial liquid trapped between them and the substrate, the latter playing the crucial role in cell adhesion.[36,37] To rule out the possibility that substrate surface wettability is the cause of the difference in cell behavior, contact angle measurements were undertaken (Figure 2i), indicating straightforward hydrophilicity (contact angle < 90°) independent of substrate composition when incubated in cell culture medium.[38] Taken together, these results indicate that substrate dissipation plays a crucial role in cell anchorage independent of elastic modulus and surface wettability.

After adhesion by integrins, cells respond to substrate mechanics through the generation of forces.[39] To understand how MG63 probe surrounding milieu in the early stages of cell-substrate interplay, we precisely inhibited actomyosin contractility using blebbistatin (inhibitor of myosinII ATP-ase) and cytochalasin D (inhibitor of actin polymerization) (**Figure 3**a,b). Additionally, MG63 cells were incubated in the presence of β-1 and β-3 integrin blocking antibodies (Figure 3c). Cell number per surface area and cell spreading area progressively lower while increasing inhibitor amount or perturbing cell binding sites. Given the relationship with the actin-myosin-integrin axis via the Rho/ROCK pathway,[40] we additionally investigated the role that microtubules play in cell adhesion process. MG63 plated on non-dissipative substrates were incubated in the presence of paclitaxel and nocodazole, a microtubule

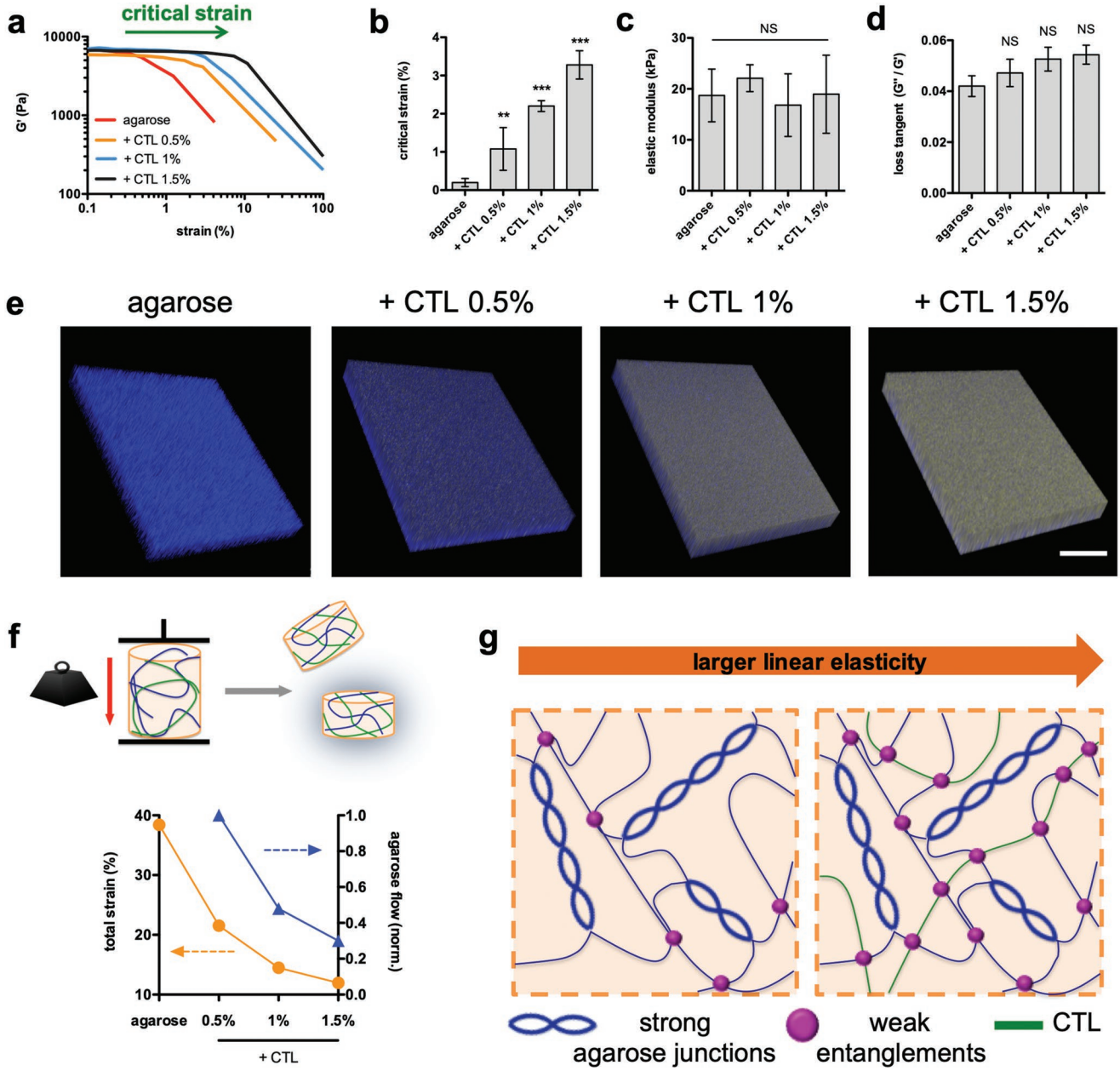

Figure 1. Development of semi-interpenetrating substrates of agarose incorporating an uncrosslinked lactose-modified chitosan (CTL) to modulate linear elasticity independent of elastic modulus and viscoelasticity. a) Elastic modulus, *G′*, profiles on applied shear strain for substrates with different composition; strain sweep experiments were performed under a constant frequency of 1 Hz. b) Critical strain at which strain softening originates; critical strain was determined according to the Soskey–Winter model (Appendix S2, Supporting Information). c) Initial elastic modulus from uniaxial compression measurements. d) Loss tangent at 0.1 Hz from frequency sweep tests. All substrates were assembled in PBS buffer, pH 7.4, with constant agarose (1% w/v) and variable CTL (0–1.5% w/v) amounts. Data are reported as mean ± s.d., $n = 5$–8 hydrogels analyzed for each experimental condition. Statistics: $^{**}p < 0.01$; $^{***}p < 0.001$; NS, not significant (one-way ANOVA followed by Dunnett's or Tukey's Multiple Comparison post hoc test). e) Confocal fluorescence microscopy of internal architecture of substrates with different composition; the scale bar is 20 µm. f) Schematic of experimental setup employed to understand tunable linear elasticity of substrates. Total strain upon constant loading and agarose amount in the bottom section of substrates after cutting; data are reported as mean, $n = 3$–6 hydrogels analyzed for each experimental condition. g) Cartoon depicting how adding uncrosslinked CTL to agarose network increases the number of weak physical entanglements (purple dots) between the polymer chains. This approach allows the elastic modulus to be kept constant due to the strong agarose junctions and it is predicted to increase the applied load to release the entanglements and thus extend the linear elasticity.

stabilizing and depolymerizing agent, respectively (Figure 3d). While the effect of paclitaxel is negligible, nocodazole elicites ≈30% reduction of cell number per substrate surface area. Whatever the perturbing agent or substrate type used to modulate cell anchorage, a significant correlation with cell spreading emerges (Spearman's rank correlation, $r = 0.898$) (Figure 3e).

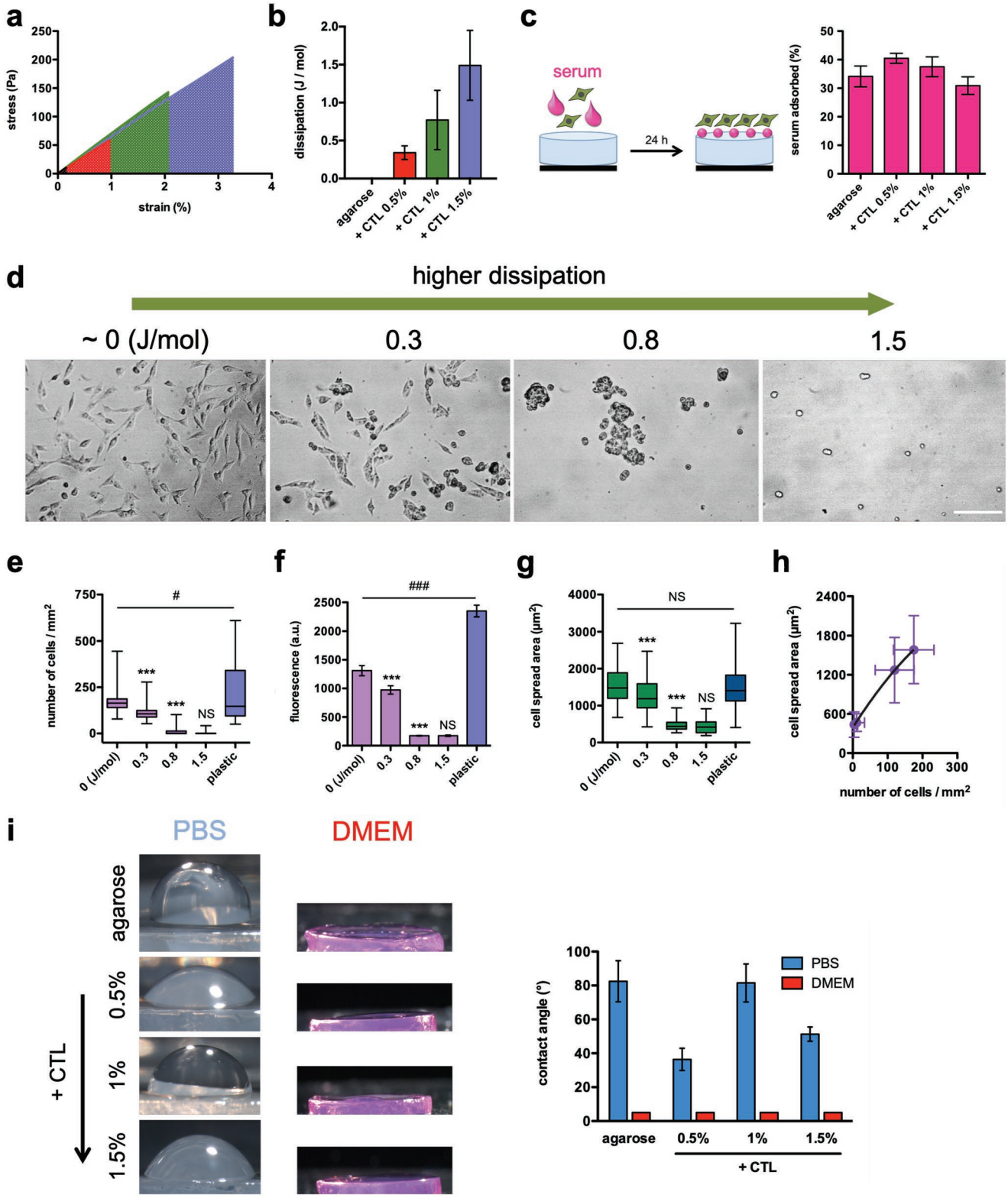

Figure 2. Substrate dissipation controls cell anchorage irrespective of elastic modulus and surface hydrophilicity. a) Representative shear stress–strain curve profiles of substrates with different composition. Data are displayed up to the critical strain at which linear elasticity ends. Dotted areas represent the energy per unit volume generated by shear to release the weak entanglements. b) Dissipation values are computed by normalizing the energy per unit volume at critical strain to the substrate crosslinking density (Appendix S4, Supporting Information for further details); data are reported as mean ± s.d., n = 5–7 hydrogels analyzed for each experimental condition, PBS buffer as solvent, pH 7.4. c) Schematic of protocol for seeding MG63 cells in the presence of serum proteins. Serum proteins adsorbed atop substrates surface were quantified through UV spectroscopy (Figure S6, Supporting

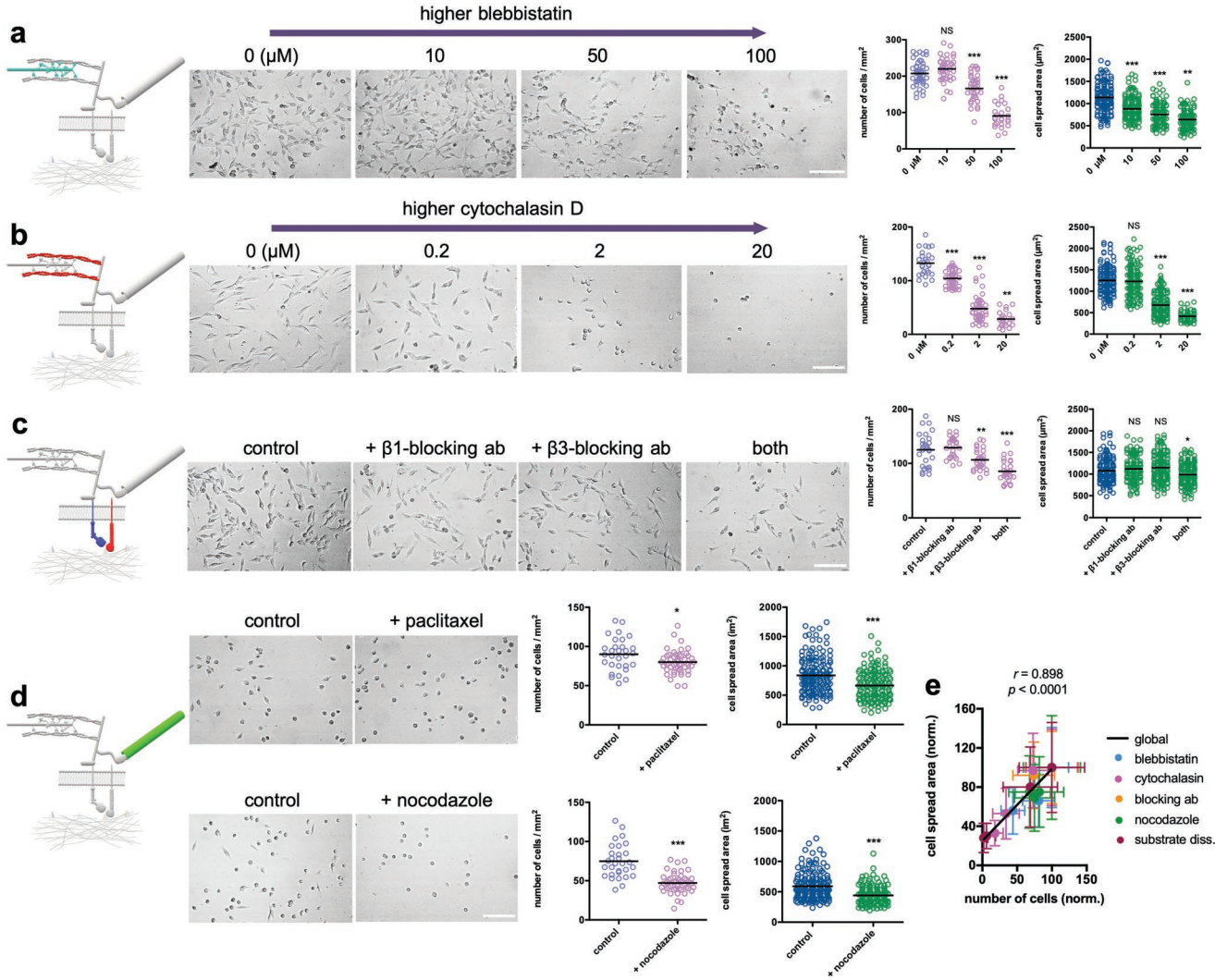

Figure 3. Cells harness actin-myosin-integrin axis to anchor the substrate but require microtubule tension. Representative images of MG63 adhering atop non-dissipative substrates (≈0 J mol^{-1}) following treatment with chemical inhibitors or blocking antibodies. Cells were incubated in the presence of a) blebbistatin, b) cytochalasin D and c) integrin blocking antibodies for 24 h, whereas 4 h in the case of d) paclitaxel and nocodazole; at the end of experiment, total cell number/substrate area, and cell spread area were determined. Data are reported as mean ± s.d., n = 23–50 images analyzed for the determination of cell number and n = 50–170 cells for computing cell spreading. Statistics: *$p < 0.05$; **$p < 0.01$; ***$p < 0.001$; NS, not significant (one-way ANOVA followed by Dunnett's or Tukey's Multiple Comparison post hoc test in (a–c); unpaired two-tailed t-test in (d). Scale bar is 200 μm in all images. e) Cell spread area as a function of cell number per surface area follows an almost linear correlation for all experimental conditions explored (Spearman's rank correlation, $r = 0.898$, $p < 0.0001$).

Taken together the observations reported in Figures 2,3, we can conclude that cell anchorage is governed by substrate dissipation linked to linear elasticity, which is mediated by the same machinery operating in cell spreading (actin-myosin-integrin axis) and requires microtubule tension.

2.3. Anchoring of Cells atop Dissipative Substrates can be Fully Compensated Upon Increasing Cell-Binding Sites

Cells transmit forces toward underlying substrate and gauge the feedback to make their fate decisions depending on the

Information); data are reported as mean ± s.d., n = 6 samples analyzed for each experimental condition. d) Representative images of MG63 adhering atop substrates with different dissipation but same elastic modulus (≈19 kPa); scale bar is 200 μm. e–g) Total cell number/substrate area, fluorescence generated by adherent MG63 cells and cell spread area for substrates with different dissipation and traditional plastic culture, the latter used as control. Data are reported as mean ± s.d., n = 28–50 images analyzed in (e), n = 5 replicates for substrate type in (f), and n = 90–230 cells in (g). Statistics: $^{\#}p < 0.05$; ***, $^{\#\#\#}p < 0.001$; NS, not significant (one-way ANOVA followed by Tukey's Multiple Comparison post hoc test). h) Correlation plot of cell spread area versus cell number/substrate area; solid black line was drawn to guide the eye. i) Representative images of water droplets atop substrates with different composition in PBS buffer or equilibrated for 24 h at 37 °C in cell culture medium (DMEM) supplemented with serum. The plot recapitulates contact angle results upon image processing; data are reported as mean ± s.d., n = 6–12 droplets analyzed in PBS and n = 3 in DMEM-equilibrated conditions.

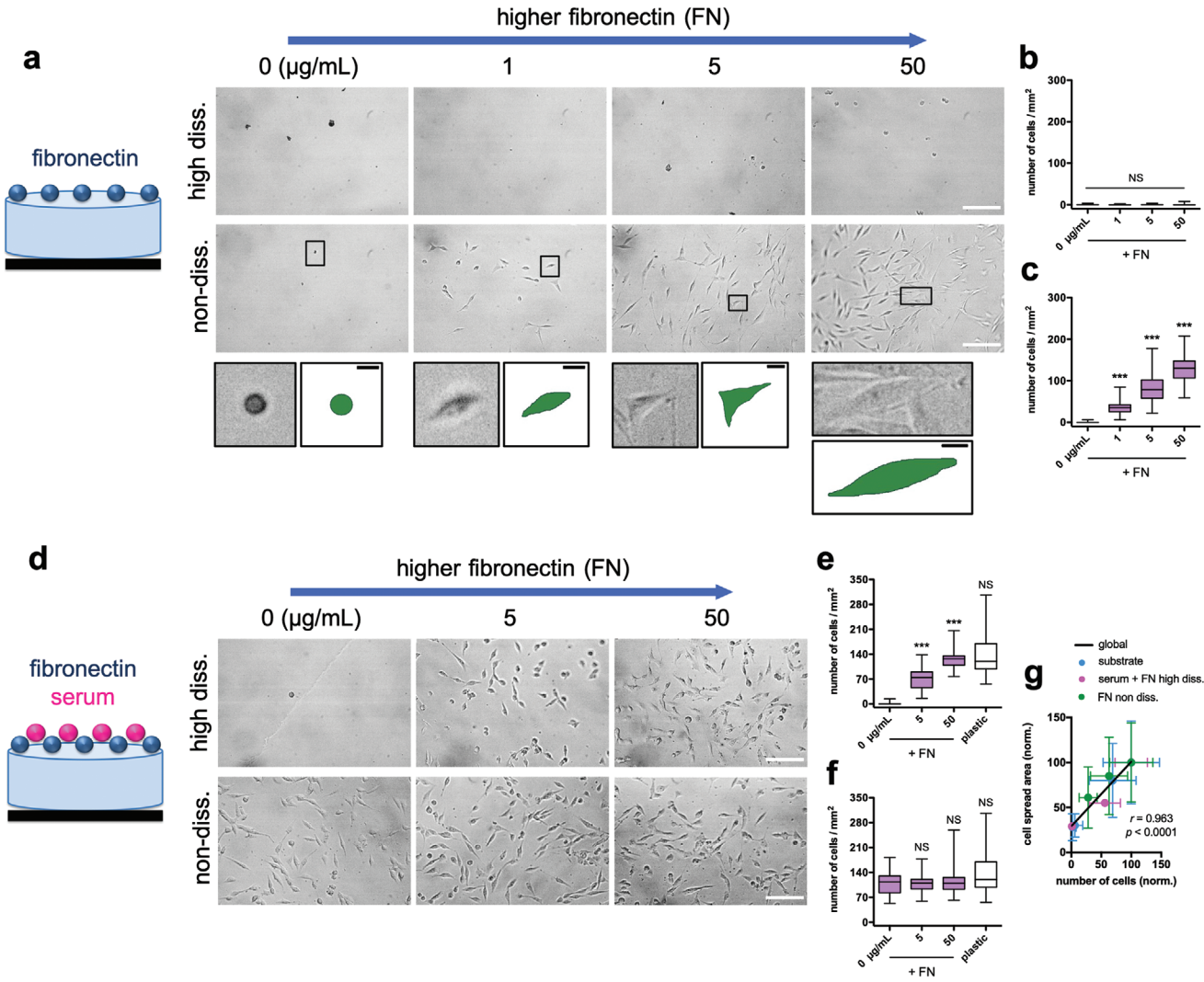

Figure 4. Cells can conceal dissipation to anchor the substrate if the amount of ligands increases. Experimental setup 1: cell seeded on fibronectin-coated substrates without serum proteins. a) Representative images of MG63 atop non-dissipative (≈0 J mol^{-1}) and high dissipative (1.5 J mol^{-1}) substrates upon increasing fibronectin. b,c) Total cell number/substrate area. Data are reported as mean ± s.d., n = 48–50 images analyzed. Statistics: $^{***}p < 0.001$; NS, not significant (one-way ANOVA followed by Tukey's Multiple Comparison post hoc test). Scale bar is 200 µm in all images. The gradual change of cell spreading upon increasing fibronectin is reported in the insets (scale bar is 20 µm). Experimental setup 2: cell seeded on fibronectin-coated substrates with serum proteins. d) Representative images of MG63 atop non-dissipative and high dissipative substrates upon increasing fibronectin in the presence of a constant amount of serum proteins. e,f) Total cell number/substrate area. Traditional plastic culture was used as a control. Data are reported as mean ± s.d., n = 28–50 images analyzed. Statistics: $^{***}p < 0.001$; NS, not significant (one-way ANOVA followed by Tukey's Multiple Comparison post hoc test). Scale bar is 200 µm in all images. g) Cell spread area as a function of cell number per surface area follows a significant correlation for all experimental conditions explored (Spearman's rank correlation, $r = 0.963$, $p < 0.0001$).

amount of anchoring points.[9,41] Therefore, we wondered whether there was a correlation between the number of ligands and substrate dissipation. First, the amount of anchoring points was systematically manipulated by the addition of the extracellular matrix protein fibronectin to the substrates. MG63 seeded atop substrates with diverse dissipation using a serum-free culture medium respond differently. While the cells do not anchor on the dissipative substrate, they progressively adhere and spread on the non-dissipative counterpart as expected (**Figure 4**a–c; Figure S8, Supporting Information). Second, MG63 were plated on fibronectin-coated substrates in the presence of serum proteins to increase the number of cell-binding sites. Here, cells completely suppress the dissipation associated with the substrate upon increasing fibronectin, hence anchoring and spreading likewise under plastic-cultured conditions (Figure 4d–f; Figure S9, Supporting Information). Importantly, a significant master curve describes the relationship between the amount of cell binding sites and substrate dissipation (Spearman's rank correlation, $r = 0.963$) (Figure 4g). On the whole, these results indicate that increasing the number of anchorage sites represents a cunning ploy to overcome substrate dissipation and thus promote cell adhesion growth.

2.4. Substrate Dissipation Impacts on Cell Migration Mode, Focal Adhesion Geometry, and Mechano-Transmission/ Transduction Processes

We then examined the effects of substrate dissipation on cell migration. Live cell microscopy was used to track MG63 on non-dissipative and dissipative substrates. Sample migrating cells recorded after 120 min of seeding show two modes of migration depending on substrate type (**Figure 5**a,b; Videos S1, S2, Supporting Information). Migration tracks display that the cells follow a zigzag or nearly linear trajectory on non-dissipative and dissipative substrates, respectively. Determination of the cell circularity parameter shows that cells prefer to migrate with rounded morphology on dissipative substrates up to ≈500 min before they begin to firmly anchor and spread, while cell polarization in the direction of migration is noticed on non-dissipative substrates (Figure 5c). This is accompanied with greater speed but less spreading observed for migrating MG-63 on dissipative substrates (Figure 5d).

From a mechanotransduction perspective, we next investigated whether substrate dissipation affected the assembly of focal adhesions and nuclear translocation of YAP. Vinculin-rich mature focal adhesions with a belt-like geometry are observed at the trailing edge of cells on non-dissipative substrates, whereas dot-like structures are evident in MG-63 on dissipative counterparts (Figure 5e). This is supported by punctate β-1 integrin structures in cells on non-dissipative substrates, reminiscent of mature focal adhesions (Figure S10, Supporting Information). Quantification of vinculin shows straightforward differences between the two systems, with a larger adhesion area observed for cells on non-dissipative substrates (Figure 5e). Furthermore, actin distribution results distinct, with stress fibers localized throughout the cytoplasm and actin bundles confined at cell periphery for cells on non-dissipative and dissipative substrates, respectively. Interestingly, the sensor YAP preferentially translocates in the nucleus for MG-63 on non-dissipative substrates (Figure 5f), indicating a different downstream response in how cells perceive substrate dissipation as mechano-regulator. In addition, we embedded fluorescent beads in the substrates to investigate the outward transmission of forces exerted by the cells. Using live imaging microscopy experiments we were able to create 3D maps showing the qualitative displacement of the beads in single stacks on dissipative and non-dissipative substrates (Figure 5g). While the fluorescent beads continued to accumulate toward the cell-substrate interface over time in the case of non-dissipative substrates, a modest movement of the beads was detected in the same time period for dissipative counterparts. Calculation of the *m* factor, which is indicative of cell traction (pulling) forces exerted by the cells, reveals unambiguous differences between the two materials analyzed. Together, these results indicate that substrate dissipation promotes cell migration with rounded morphology, associated with smaller dot-like anchoring points, greater speed, less pulling forces generated by the cells, and less nuclear translocation of YAP.

3. Discussion

In summary, this work unveils an unprecedented approach to the development of 2D viscoplastic substrates with tunable linear elasticity, fast stress relaxation, and similar elastic modulus (Figure 1). Nonetheless, our findings establish dissipation associated with linear elasticity as a potent controller directing cell-substrate interplay. Although recent works have reported the physical entrapment of a very high molecular weight linear polyacrylamide in a purely elastic material or partial crosslinking strategy to modulate viscous dissipation,[16–18] our approach is unique for two main reasons: i) the assembly of semi-interpenetrating networks by temperature-assisted gelation of agarose without the addition of crosslinkers; ii) the release of weak entanglements to dissipate the load independent of viscoelasticity. Widely, our experimental approach allows to readily fabricate 3D extracellular matrix mimics as model to build fundamental knowledge about the influence of linear elasticity—and ensuing dissipation—on cell behavior.

In this work we have exploited this set of materials to decipher how cells probe the underlying substrate and decide whether and how to anchor or not. Our results reveal that cells exert traction forces through the actin-myosin-integrin molecular clutch but require microtubule tension to adhere firmly (Figure 3). Substrate dissipation yields a crucial material trait (Figure 2), but can be completely suppressed if the amount of ligands is increased (Figure 4). This evidence supports the intriguing vision that a strict correlation between substrate dissipation, number of cell-binding sites, and cytoskeletal architecture does exist. While the materials used in this study differ in stress relaxation response, the latter is fast (tens of seconds). The agarose/CTL substrates therefore accurately recapitulate the rapid timescale of cell dynamics and the range of dissipation (0–1.5 J mol^{-1}) for initial cell mechanosensing.[21,42,43] In this regard, nascent adhesion points with size ≈0.2 μm^2 build up and turnover in discrete phases on glass dishes, entailing assembly, stability, and disassembly in a timescale of 20–100 s. Maturation then occurs slowly in a time frame of a few minutes along an α-actinin-actin template extending centripetally from the nascent adhesions, with actin cross-linking by myosin II playing an important role in this process.[44] Molecular clutch dynamics occurs in the range of seconds on viscoelastic or relative elastic hydrogels and manifests a stiffness and viscoelasticity sensing.[6,7,14,45] The question of how adhesion points on viscoplastic substrates with adjustable linear elasticity and fast stress relaxation in the range of tens of seconds, as in our case, are assembled in relatively short periods of time is a more difficult question that remains to be answered.

While viscosity has been found to have an effect on cell adhesion growth,[16,18] it is important to recall that dissipation in our materials is related to the extent of linear elasticity due to the release of weak entanglements, not viscosity, and cells respond to this material trait. A recent study has shown that viscosity serves to stiffen soft viscoelastic substrates on a timescale faster than the clutch off-rate, which enhances cell spreading. In contrast, viscosity does not influence cell spreading in relative stiff substrates, since the bound clutches are saturated by the elevated stiffness.[14] Our substrates are viscoelastic and are relative stiff (≈19 kPa), thus it is to be expected that viscosity plays a negligible role in cell response. Hence, it results attractive to envisage that cells, upon binding protein ligands, probe the substrate via rapid pulling/pushing mechanics where both actomyosin and microtubules tensors are involved in these

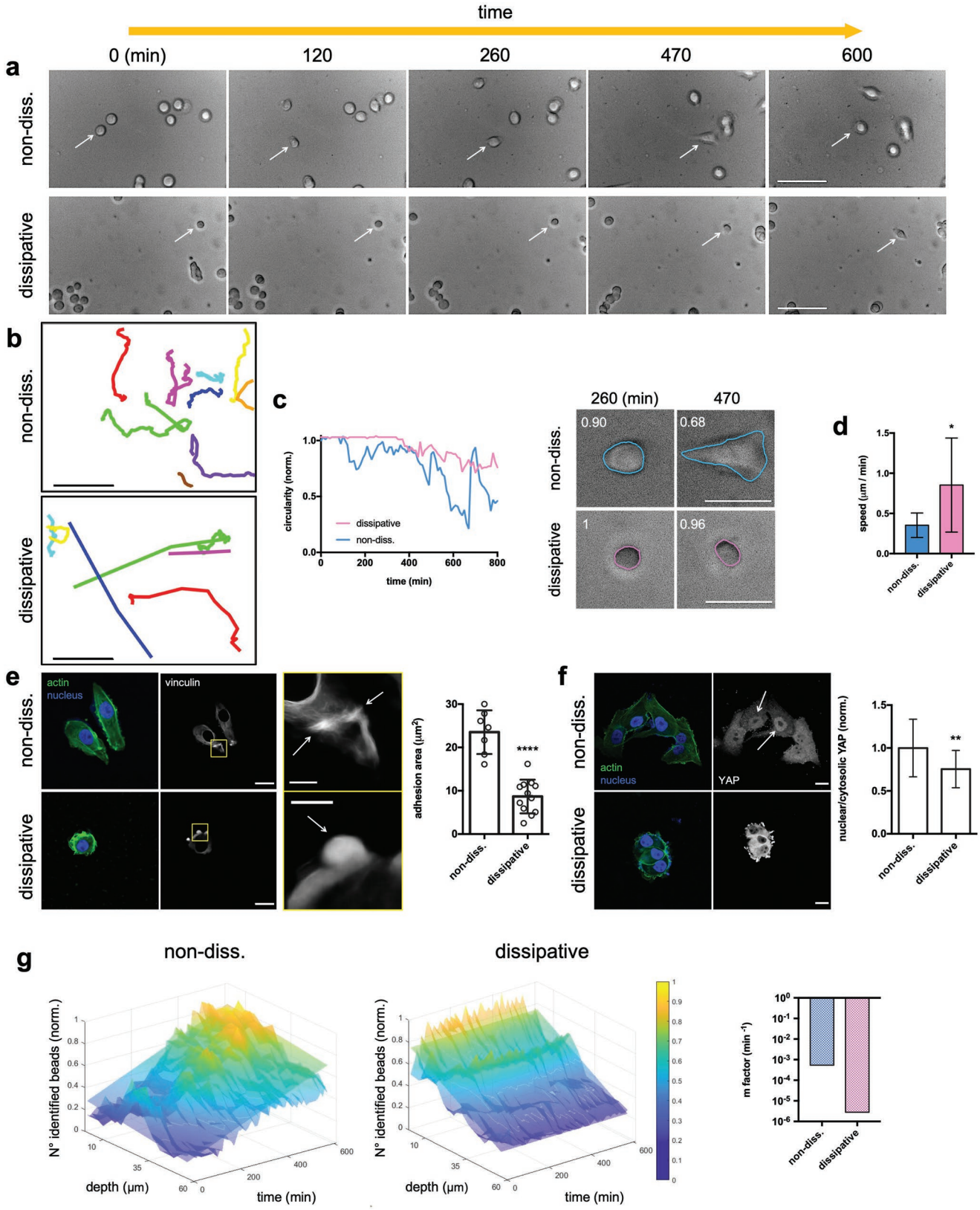

Figure 5. Substrate dissipation directs cell migration with rounded morphology through dot-like anchoring points, greater speed but less pulling forces exerted by cells. a) Bright field images of migrating MG63 over time on non-dissipative (≈0 J mol^{-1}) and dissipative (0.3 J mol^{-1}) substrates. Note that images are reported after 120 min of cell seeding. MG63 has been plated in the presence of serum proteins and without fibronectin coating. Scale bars

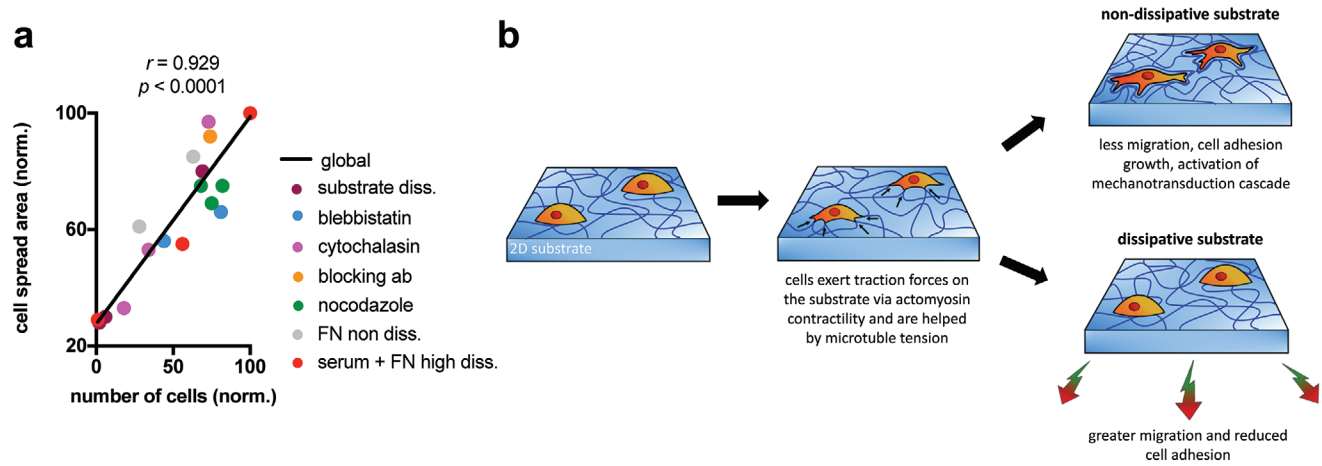

Figure 6. Cell activity on 2D cultures is controlled by substrate dissipation linked to linear elasticity. a) Cell spread area as a function of cell number per surface area follows a significant correlation for all different experimental conditions examined in this study (Spearman's rank correlation, $r = 0.929$, $p < 0.0001$). b) Cartoon schematic recapitulating what identified in this study. After substrate anchoring, cells exert traction forces via the actin-myosin-integrin axis and helped by microtubules tension. In fast stress-relaxing and non-dissipative material, cells sense the mechanical feedback from the substrate, which triggers the activation of the mechanotransduction cascade and causes adhesion growth; this is associated with reduced cell migration and is thought to be associated with matrix remodeling. For fast stress-relaxing and dissipative material, force transmission is partially dissipated through the substrate and mechanical feedback is expected to be lower. This promotes greater cell migration but less anchorage and spreading. Importantly, substrate dissipation can be completely suppressed when the amount of cell-binding sites is increased, indicating a correlation between force transmission, substrate dissipation rate, and the number of anchoring points.

timescales.[1] Starting now, substrate dissipation linked to linear elasticity intervenes as key actor directing cell fate decisions (**Figure 6**). When dissipation is set very low, force transmission is almost completely converted to a feedback response,[41] promoting mechanotransduction events entailing maturation of vinculin-dependent focal adhesions, YAP nuclear translocation, and highly spread morphologies (Figure 5). Instead, when dissipation is set high, force transduction occurs only upon increasing extracellular matrix sites tethering, thereby concealing substrate mechanics and promoting true adhesion growth (Figure 4).

In addition, substrate dissipation impacts on cell migration mode (Figure 5). Typical lamellipodia-mediated migration[46,47] at the leading edge on non-dissipative substrates, whereas rounded-morphology associated with greater speed on dissipative counterparts is seen, likewise what observed in different cancer cell lines on soft viscoelastic substrates.[48] How dissipation mediates cell migration on relatively stiff viscoplastic substrates is a more challenging question that remains to be answered, but it is tempting to speculate that nascent adhesions together with filopodia protrusion might jointly contribute.

In contrast to purely elastic substrates, which have a threshold of stiffness that marks the onset of massive traction forces exerted by cells, YAP nuclear translocation and the growth of focal adhesions rich in vinculin,[9] our substrates manifest same stiffness and show plasticity (Figure S3, Supporting Information) likewise reconstituted ECM materials based on type-1 collagen, fibrin, and basement membrane matrix.[2,49] Here, live imaging microscopy allowed us to understand that cells generate much more traction (pulling) stresses on non-dissipative substrates associated with cell spread morphology (Figures 2,5). It is possible that a correlation between substrate plasticity and spreading speed exists at a very low dissipation rate (≈0 vs 0.3 J mol^{-1}).[50] However, our findings show that cell anchorage is completely suppressed at a high dissipation rate (>0.8 J mol^{-1}), low ligand amount, and comparable substrate plasticity (≈20%). Moreover, substrates with different dissipation exhibit fast stress relaxation. This suggests that cells transduce biophysical cues on relatively similar time scales. Instead of a threshold for stiffness, this body of evidence again justifies the existence of a threshold for dissipation in the case of viscoplastic substrates. Hence, when the dissipation threshold is exceeded, the cells exert high traction forces and spread. If the dissipation threshold is not exceeded, the cells exert less traction forces and spread less. It will be interesting to see the results of future studies on how cell mechanotransmission correlates with matrix remodeling for this set of substrates. Broadly, this study confirms that dissipation represents a paramount feature to consider for investigating cell mechanosensing both in 2D and in 3D experimental conditions, and

are 100 µm. b) Migration tracks of randomly selected MG63 on indicated substrates over a timescale of ≈800 min. Scale bars are 100 µm. c) Circularity plot profile over time (left) and representative images of migrating MG63 cells (right) on indicated substrates. The circularity parameter is reported in the upper left corner for each image. Note that circularity equal to 1 refers to almost perfectly rounded cells. Scale bars are 100 µm. d) Cell migration speed on non-dissipative and dissipative substrates. Data are reported as mean ± s.d., $n = 4$–9 cells analyzed. Statistics: $^{*}p < 0.05$ (unpaired Mann–Whitney t-test). Immunostaining and quantification of e) vinculin and f) YAP for MG63 cells on non-dissipative and dissipative substrates. Data are reported as mean ± s.d., $n = 7$–12 cells analyzed in (e) and $n = 20$–35 in (f). Statistics: $^{**}p < 0.01$; $^{****}p < 0.0001$ (Student's t-test). Scale bars are 20 µm, zoom-in/inset 5 µm. g) 3D intensity maps showing fluorescent beads (normalized) position within 60 µm-depth for non-dissipative and dissipative substrates over a time scale of 600 min. Note that 0 µm indicates the outermost substrate layer, that is the cell–substrate interface. The slope over time (m factor) of the regression plane, indicative of cell traction (pulling) forces exerted by cells, is reported in the bar plot.

introduces linear elasticity as a design parameter in the fabrication of materials with adjustable dissipation rates.

4. Experimental Section

Substrates Preparation: Hydrochloride lactose-modified chitosan, CTL, was kindly provided by biopoLife, (Italy). The chemical composition of CTL resulted: fraction of deacetylated units (F_D) 0.21, fraction of lactose-modified units (F_L) 0.63, and fraction of acetylated units (F_A) 0.16. The calculated molar mass of CTL repeating unit ($MW_{r.u.}$)—given its chemical composition—resulted 403 g mol^{-1}. The intrinsic viscosity, [η], was 344 mL g^{-1} and the related molar mass was around 800 000 g mol^{-1}.[31] Different amounts of CTL powder were dissolved in deionized water. The pH was adjusted to 7.4 and 10× phosphate buffered saline (PBS, Sigma, USA) added. Final experimental conditions are the following: [CTL] = 0–1.5% w/v, 1× PBS as solvent, pH 7.4 (see Supporting Information for further details). Agarose LE powder (code EMR920500) with gelling temperature 36 ± 1.5 °C (Euroclone, Italy) was next added to CTL solutions under vigorous stirring to have a final concentration of 1% w/v. Resulting mixtures were autoclaved and dispensed into cylindrical supports prior cooling down at room temperature. Substrates were finally incubated overnight at 37 °C in water-saturated conditions to prevent solvent evaporation.

Mechanical Characterization: Rheological characterization of substrate disks (20 mm in diameter, 2–2.5 mm thick, PBS buffer or cell culture medium-equilibrated conditions) was performed by means of a controlled stress rheometer HAAKE MARS III operating at 37 °C using a shagreened plate-plate apparatus ("HPP20 profiliert": diameter = 20 mm) as the measuring device. To avoid water evaporation from substrates, measurements were performed in a water-saturated environment formed by using a glass bell (solvent trap) containing a wet cloth. In addition, to prevent both wall-slippage and excessive substrate squeezing, the gap between plates was adjusted by executing a series of short stress sweep tests ($\nu = 1$ Hz; stress range 1–5 Pa) until a constant G' was reached. The linear viscoelastic range was determined by means of stress sweep tests consisting in measuring the elastic (G') and viscous (G'') moduli variation with increasing shear stress (1 Pa < τ < 1000 Pa) at a frequency $\nu = 1$ Hz (hence with $\omega = 2\pi\nu$ = 6.28 rad s^{-1}). The mechanical spectra (frequency sweep tests) were recorded by measuring the dependence of the elastic (G') and viscous (G'') moduli on pulsation frequency at constant shear stress $\tau = 5$ Pa (well within the linear viscoelastic range). Quantification of substrate plasticity was determined by creep-recovery measurements with τ = 100 Pa for 900 s followed by $\tau = 0$ Pa for 900 s. The degree of plasticity was calculated as previously described.[49]

Uniaxial compression of substrate disks (20 mm in diameter, 2–2.5 mm thick, PBS buffer or cell culture medium-equilibrated conditions) was performed by means of a universal testing machine (Mecmesin Multitest 2.5-i) equipped with a 100 N load cell. A compression speed of 1 mm min^{-1} was applied to determine initial elastic modulus in the strain range 1–3%. Stress relaxation tests were conducted by applying a constant strain of 15% for 600 s. The time needed to relax the stress to half of the initial value, $\tau_{0.5}$, was considered as parameter to compare substrates with different composition.[24]

Structural Characterization: The distribution of agarose and CTL throughout substrates was analyzed by confocal microscopy (Nikon Eclipse C1si confocal laser scanning microscope using a 40× as objective). Substrates were assembled using 10% w/w of FITC (Sigma, USA)-labeled CTL and 10% w/w of Atto Rho101 NHS ester (Sigma, USA)-labeled agarose. Protocols describing polymer labeling procedures are reported in Appendix S3, Supporting Information. Substrates were sectioned and the fluorescent signals acquired. Resulting stacks of images were analyzed using Fiji-ImageJ software to develop 3D renderings of the inner part of substrates with different composition. The distribution of agarose and CTL throughout substrates upon mechanical stimulation was analyzed by ^{1}H-NMR. Uniaxial compression of substrate cylinders (16 mm in diameter, 8 mm thick, PBS buffer) was performed with a compression speed of 1 mm min^{-1} up to achieving a load of 0.6 N (3 kPa). The load was then kept constant for 15 min. At the end of experiment the cylinders were gathered, cut in two pieces and the bottom section frozen and lyophilized. Freeze-dried samples were next dissolved in warm D_2O ($T \approx 95$ °C) and finally transferred into NMR tubes. ^{1}H-NMR spectra were recorded by means of a 400 VNMRS Varian NMR spectrometer operating at 400 MHz. Prior to the measurement, samples were heated to 93 °C for 5 min and then kept at 60 °C during the NMR analyses.

Swelling and degradation properties of substrates were verified after 1 and 7 days of incubation in cell culture medium at 37 °C. At the end of incubation, substrates were laid down on filter papers to blot the excess of medium, weighed, frozen, and lyophilized. The dry mass of substrates was finally recorded.

Evaluation of Surface Wettability: Contact angle on substrates with different composition were measured by means of an optical stereomicroscope (MZ16, Leica Microsystems GmbH) equipped with a digital camera (DFC320, Leica Microsystems GmbH) and a 45° tilted mirror. A droplet of deionized water (4 µL) was placed atop substrates surface and let to rest for 1 min. The profile of water droplet was next recorded. Image-Pro Plus 6.2 software (Media Cybernetics, Inc.) was used to acquire, process the images, and measure the contact angle. Substrates were analyzed in PBS buffer or cell culture medium-equilibrated conditions and room temperature.

Cell Culture: Human osteosarcoma MG63 (ATCC CRL-1427) were cultured in Dulbecco's Modified Eagle's Medium High glucose with 0.584 g L^{-1} L-glutamine and 0.11 g L^{-1} sodium pyruvate (EuroClone, Italy), supplemented with 10% heat-inactivated fetal bovine serum (Cat. n° ECS0180L, Euroclone, Italy) and 1% penicillin/streptomycin (EuroClone, Italy), in a humidified atmosphere of 5% CO_2 at 37 °C.

Plating of Cells atop Substrates: Upon autoclaving, agarose/CTL mixtures were transferred into a water bath pre-warmed at 60 °C and let at rest for 10 min. Next, 400 µL of mixtures were dispensed into 24-well plates and let at rest for 30 min at room temperature to promote gelation. Substrates were finally incubated overnight at 37 °C in water-saturated conditions. For fibronectin-coated experiments, substrates were additionally incubated overnight at 4 °C with 300 µL of fibronectin (Sigma, USA) dispersed in PBS. The day after PBS was discarded and substrates washed by cold PBS. Cells were trypsinized and plated at a density of 30 000 cells per well using 1.6 mL of cell culture medium/well supplemented or not with fetal bovine serum, hence the final V_{PBS}/V_{medium} ratio resulted 20:80 v/v. Cells were incubated overnight in a humidified atmosphere of 5% CO_2 at 37 °C.

Assessment of Cell Adhesion and Spreading: After overnight incubation, cell culture medium was discarded and substrates were washed extensively with PBS in order to remove non-adherent cells. Then, 300 µL per well of PBS were added and the number of adherent cells mm^{-2} and cell spread area were quantified by Fiji-ImageJ software (multi-point and freehand selection tools, respectively) from 1000 µm × 700 µm images acquired through a Exacta Optech microscope equipped with a Pentax digital camera using a 10× as objective. PBS was next discarded and cells incubated furthermore with 200 µL per well of AlamarBlue reagent (Sigma, USA), 10% v/v in complete DMEM medium for 4 h at 37 °C. At the end of incubation, 150 µL of incubation medium were transferred in a black 96-well plate and the fluorescence was measured using a FLUOStar Omega-BMG Labtech spectrofluorometer (λ_{ex} = 544 nm; λ_{em} = 590 nm).

Blocking Adhesion Experiments: Cells were plated at a density of 30 000 cells per well using 1.6 mL of cell culture medium/well supplemented with fetal bovine serum in the presence of following chemicals: (±)-blebbistatin (10–100 µM, Santa Cruz Biotechnology), cytochalasin D (0.2–20 µM, Santa Cruz Biotechnology), paclitaxel (0.2 µM, Sigma), and nocodazole (10 µM, Sigma).[19,21,40,51] Furthermore, cells were incubated with mouse anti-human integrin β-1 monoclonal antibody (5 µg mL^{-1}, clone P5D2, Catalogue no. MAB1959, Merck, Germany) and mouse anti-human integrin β-3 monoclonal antibody (5 µg mL^{-1}, Catalogue no. MAB2023Z, Merck, Germany). Substrates were then incubated for

4 or 24 h in a humidified atmosphere of 5% CO_2 at 37 °C. At the end of experiment, the substrates were washed extensively with PBS in order to remove non-adherent cells, processed for image acquisition, and incubated with the AlamarBlue mixture as described above.

Cell Immunostaining and Image Analysis: After overnight incubation, cell culture medium was discarded and substrates washed extensively with PBS in order to remove non-adherent cells. Then, substrates were punched into small disks (9 mm in diameter, 2.5 mm thick) and moved in clean 48-well plate. Cells were fixed with formaldehyde 4% v/v (Sigma, USA) in PBS for 30 min at room temperature. Then, substrates were washed 5× with PBS and permeabilized with Triton 0.2% v/v (Sigma, USA) in PBS for 15 min at room temperature. Next, substrates were washed with PBS and incubated with BSA 4% w/v (Sigma, USA) + Normal Goat Serum 5% v/v (Sigma, USA) in PBS for 1 h at 37 °C. The blocking solution was then removed and the samples washed with PBS. The following primary antibodies were used for immunostaining: YAP antibody (dilution 1:200 or 0.5 μg mL^{-1}, sc-101199, Santa Cruz), integrin β-1 antibody (dilution 1:200 or 1 μg mL^{-1}, sc-9970, Santa Cruz), and vinculin antibody (dilution 1:200 or 5 μg mL^{-1}, V9264, Sigma). Primary antibodies were diluted in blocking mixture. In the case of YAP, Triton 0.1% v/v was also added to blocking mixture. Incubation was proceeded overnight at 4 °C. Then, cells were washed and incubated with secondary antibody Mouse IgGk light chain diluted in blocking solution (dilution 1:250 or 1.6 μg mL^{-1}, sc-516179, Santa Cruz) for 2 h at room temperature. For the visualization of F-actin filaments and nuclei, cells were counterstained with Phalloidin Fluorescein Isothiocyanate Labeled (P5282, Sigma, 1 μg mL^{-1} in PBS) and Hoechst (33258, Invitrogen, 5 μg mL^{-1} in PBS), respectively. Finally, substrates were washed once and stored in PBS. Images from immunofluorescence and cellular staining experiments were acquired using a Nikon C1si confocal microscope (Nikon, Tokyo, Japan), containing 488 (argon), 408, and 561 nm (diode) lasers. Light was delivered to the sample with an 80/20 reflector. The system was operated with a pinhole size of one Airy disk. Electronic zoom was kept at minimum values for measurements to reduce potential bleaching. For the different fields collected 60× Plan Apo objectives were used, saving series of optical images respectively at 160 μm × 160 μm with 0.4 μm z-resolution step size. Images in various conditions were captured under identical acquisition settings in order to allow comparison of fluorescent intensity and were processed for maximum z-projection by using Fiji-ImageJ 1.53c (NIH, Bethesda, USA). The staining quantification was performed and analyzed by the ImageJ tool ROI manager. The degree of YAP nuclear localization was assessed as previously described.[9]

Cell Migration Experiments and Pulling Force Measurements: Substrates were assembled in 24-well plate in the presence of 0.2% v/v carboxylate-modified FluoSpheres (0.2 μm, red 580/605, Invitrogen). Cells were trypsinized and plated at a density of 100 000 cells per well using 1.6 mL of cell culture medium/well supplemented with fetal bovine serum. Live imaging of cells was performed using a Nikon Eclipse Ti microscope equipped with incubator on stage for the control of environment parameters, temperature at 37 °C and CO_2 at 5%. The fields were acquired with a long working distance PlanApo 40× objective at the maximum camera resolution. The imaging protocol lasted 16 h with a sampling frequency of one field every 10 min. In order to account variable surface of the substrate at each time point a multiple stacks acquisition was performed for a total thickness of 120 μm with a step size of 20 μm. All videos were subsequently processed for maximum intensity projection of z-stacks at each time point and for fluorescence intensity equalized over time. Digital image processing was performed in order to segment the cells from the background. An automatic segmentation protocol composed of flat fielding, denoising, thresholding, and refinement via morphological processing was fine tuned. Segmentation was performed on the top-most layer of the brightfield channel for each available time point. Then, the centroid and the circularity of the segmented cells were computed by means of the regionprops MATLAB command. The number of identified beads was also computed and, in this case, all the slices (i.e., the different depths) of the stack of images were taken into account, thus to jointly assess both time and depth dependencies. A pulling force could be then derived as the slope (*m* factor) of the regression plane interpolating these points.

Statistical Analysis: Statistical comparisons and graphical elaborations were carried out using GraphPad Prism software. A one-way ANOVA (analysis of variance) was performed, followed by a Dunnett or Tukey post hoc test to assess differences between the different groups and the control. An unpaired Mann–Whitney two-tailed *t*-test was performed to assess differences between two groups. Differences were considered significant if the *p*-value was less than 0.05. Spearman's rank correlation test was performed to assess the significance of the data trends.

Supporting Information

Supporting Information is available from the Wiley Online Library or from the author.

Acknowledgements

The financial support to P.S. (Fellowship, project: "Preparazione mediante metodi eco-sostenibili di matrici di idrocolloidi per analisi batteriologiche e virologiche"- Bando A2/2020) by AREA Science Park is gratefully acknowledged. This work was also funded by FFABR, MIUR-University of Trieste granted to G.B. Confocal and Epifluo images reported in this article were generated in the Light Microscopy Imaging Center of the University of Trieste at the Life Sciences Department, funded as detailed at www.units.it/confocal.

Conflict of Interest

The authors declare no conflict of interest.

Author Contributions

P.S. designed and performed the experiments, analyzed and interpreted the results, and wrote the paper; F.P. performed part of mechanical investigation, carried out adhesion and spreading experiments, and helped with the discussion of results; C.P. performed most of rheological experiments; G.B. supervised confocal microscopy experiments, assisted in the set-up of live imaging recordings, and helped with the interpretation of results; F.B. carried out data analysis from live imaging experiments; E.M. provided ideas and assisted data interpretation and discussions of biological results; I.D. supervised the project, interpreted the results, and proofread the paper.

Data Availability Statement

The data that support the findings of this study are available from the corresponding author upon reasonable request.

Keywords

cell adhesion growth, cell migration, dissipation, mechanotransmission/transduction, viscoplastic substrates

Received: January 10, 2022
Revised: April 8, 2022
Published online:

[1] O. Chaudhuri, J. Cooper-White, P. A. Janmey, D. J. Mooney, V. B. Shenoy, *Nature* **2020**, *584*, 535.
[2] S. Nam, K. H. Hu, M. J. Butte, O. Chaudhuri, *Proc. Natl. Acad. Sci. USA* **2016**, *113*, 5492.
[3] S. Münster, L. M. Jawerth, B. A. Leslie, J. I. Weitz, B. Fabry, D. A. Weitz, *Proc. Natl. Acad. Sci. USA* **2013**, *110*, 12197.
[4] W. Yang, V. R. Sherman, B. Gludovatz, E. Schaible, P. Stewart, R. O. Ritchie, M. A. Meyers, *Nat. Commun.* **2015**, *6*, 6649.
[5] F. H. Silver, J. W. Freeman, G. P. Seehra, *J. Biomech.* **2003**, *36*, 1529.
[6] C. E. Chan, D. J. Odde, *Science* **2008**, *322*, 1687.
[7] B. L. Bangasser, G. A. Shamsan, C. E. Chan, K. N. Opoku, E. Tüzel, B. W. Schlichtmann, J. A. Kasim, B. J. Fuller, B. R. McCullough, S. S. Rosenfeld, D. J. Odde, *Nat. Commun.* **2017**, *8*, 15313.
[8] B. L. Bangasser, S. S. Rosenfeld, D. J. Odde, *Biophys. J.* **2013**, *105*, 581.
[9] A. Elosegui-Artola, R. Oria, Y. Chen, A. Kosmalska, C. Pérez-González, N. Castro, C. Zhu, X. Trepat, P. Roca-Cusachs, *Nat. Cell Biol.* **2016**, *18*, 540.
[10] P. Kanchanawong, G. Shtengel, A. M. Pasapera, E. B. Ramko, M. W. Davidson, H. F. Hess, C. M. Waterman, *Nature* **2010**, *468*, 580.
[11] J. Swift, I. L. Ivanovska, A. Buxboim, T. Harada, P. C. D. P. Dingal, J. Pinter, J. D. Pajerowski, K. R. Spinler, J.-W. Shin, M. Tewari, F. Rehfeldt, D. W. Speicher, D. E. Discher, *Science* **2013**, *341*, 1240104.
[12] S. Dupont, L. Morsut, M. Aragona, E. Enzo, S. Giulitti, M. Cordenonsi, F. Zanconato, J. L. Digabel, M. Forcato, S. Bicciato, N. Elvassore, S. Piccolo, *Nature* **2011**, *474*, 179.
[13] M. Cantini, H. Donnelly, M. J. Dalby, M. Salmeron-Sanchez, *Adv. Healthcare Mater.* **2020**, *9*, 1901259.
[14] Z. Gong, S. E. Szczesny, S. R. Caliari, E. E. Charrier, O. Chaudhuri, X. Cao, Y. Lin, R. L. Mauck, P. A. Janmey, J. A. Burdick, V. B. Shenoy, *Proc. Natl. Acad. Sci. USA* **2018**, *115*, E2686.
[15] M. Bennett, M. Cantini, J. Reboud, J. M. Cooper, P. Roca-Cusachs, M. Salmeron-Sanchez, *Proc. Natl. Acad. Sci. USA* **2018**, *115*, 1192.
[16] A. R. Cameron, J. E. Frith, J. J. Cooper-White, *Biomaterials* **2011**, *32*, 5979.
[17] A. R. Cameron, J. E. Frith, G. A. Gomez, A. S. Yap, J. J. Cooper-White, *Biomaterials* **2014**, *35*, 1857.
[18] E. E. Charrier, K. Pogoda, R. G. Wells, P. A. Janmey, *Nat. Commun.* **2018**, *9*, 449.
[19] O. Chaudhuri, L. Gu, M. Darnell, D. Klumpers, S. A. Bencherif, J. C. Weaver, N. Huebsch, D. J. Mooney, *Nat. Commun.* **2015**, *6*, 6365.
[20] A. Bauer, L. Gu, B. Kwee, W. A. Li, M. Dellacherie, A. D. Celiz, D. J. Mooney, *Acta Biomater.* **2017**, *62*, 82.
[21] P. Sacco, G. Baj, F. Asaro, E. Marsich, I. Donati, *Adv. Funct. Mater.* **2020**, *30*, 2001977.
[22] I. A. Marozas, K. S. Anseth, J. J. Cooper-White, *Biomaterials* **2019**, *223*, 119430.
[23] I. A. Marozas, J. J. Cooper-White, K. S. Anseth, *New J. Phys.* **2019**, *21*, 045004.
[24] O. Chaudhuri, L. Gu, D. Klumpers, M. Darnell, S. A. Bencherif, J. C. Weaver, N. Huebsch, H. Lee, E. Lippens, G. N. Duda, D. J. Mooney, *Nat. Mater.* **2016**, *15*, 326.
[25] J. Lou, R. Stowers, S. Nam, Y. Xia, O. Chaudhuri, *Biomaterials* **2018**, *154*, 213.
[26] S. Nam, R. Stowers, J. Lou, Y. Xia, O. Chaudhuri, *Biomaterials* **2019**, *200*, 15.
[27] C. Loebel, R. L. Mauck, J. A. Burdick, *Nat. Mater.* **2019**, *18*, 883.
[28] K. H. Vining, A. Stafford, D. J. Mooney, *Biomaterials* **2019**, *188*, 187.
[29] L. J. Dooling, M. E. Buck, W.-B. Zhang, D. A. Tirrell, *Adv. Mater.* **2016**, *28*, 4651.
[30] B. M. Richardson, D. G. Wilcox, M. A. Randolph, K. S. Anseth, *Acta Biomater.* **2019**, *83*, 71.
[31] P. Sacco, F. Furlani, A. Marfoglia, M. Cok, C. Pizzolitto, E. Marsich, I. Donati, *Macromol. Biosci.* **2020**, *20*, 2000236.
[32] N. D'Amelio, C. Esteban, A. Coslovi, L. Feruglio, F. Uggeri, M. Villegas, J. Benegas, S. Paoletti, I. Donati, *J. Phys. Chem. B* **2013**, *117*, 13578.
[33] P. Sacco, F. Furlani, S. Paoletti, I. Donati, *Biomacromolecules* **2019**, *20*, 3070.
[34] M. Borkenhagen, J. F. Clémence, H. Sigrist, P. Aebischer, *J. Biomed. Mater. Res.* **1998**, *40*, 392.
[35] K. Y. Lee, D. J. Mooney, *Chem. Rev.* **2001**, *101*, 1869.
[36] J. Étienne, J. Fouchard, D. Mitrossilis, N. Bufi, P. Durand-Smet, A. Asnacios, *Proc. Natl. Acad. Sci. USA* **2015**, *112*, 2740.
[37] A. Monemian Esfahani, W. Zhao, J. Y. Chen, C. Huang, N. Xi, J. Xi, R. Yang, *Anal. Chem.* **2018**, *90*, 10340.
[38] R. S. Hebbar, A. M. Isloor, A. F. Ismail, *Membrane Characterization*, Elsevier, Amsterdam **2017**, p. 219.
[39] M. A. Wozniak, C. S. Chen, *Nat. Rev. Mol. Cell Biol.* **2009**, *10*, 34.
[40] N. B. M. Rafiq, Y. Nishimura, S. V. Plotnikov, V. Thiagarajan, Z. Zhang, S. Shi, M. Natarajan, V. Viasnoff, P. Kanchanawong, G. E. Jones, A. D. Bershadsky, *Nat. Mater.* **2019**, *18*, 638.
[41] B. Trappmann, J. E. Gautrot, J. T. Connelly, D. G. T. Strange, Y. Li, M. L. Oyen, M. A. Cohen Stuart, H. Boehm, B. Li, V. Vogel, J. P. Spatz, F. M. Watt, W. T. S. Huck, *Nat. Mater.* **2012**, *11*, 642.
[42] G. Giannone, B. J. Dubin-Thaler, H. G. Döbereiner, N. Kieffer, A. R. Bresnick, M. P. Sheetz, *Cell* **2004**, *116*, 431.
[43] V. Vogel, M. Sheetz, *Nat. Rev. Mol. Cell Biol.* **2006**, *7*, 265.
[44] C. K. Choi, M. Vicente-Manzanares, J. Zareno, L. A. Whitmore, A. Mogilner, A. R. Horwitz, *Nat. Cell Biol.* **2008**, *10*, 1039.
[45] R. Oria, T. Wiegand, J. Escribano, A. Elosegui-Artola, J. J. Uriarte, C. Moreno-Pulido, I. Platzman, P. Delcanale, L. Albertazzi, D. Navajas, X. Trepat, J. M. García-Aznar, E. A. Cavalcanti-Adam, P. Roca-Cusachs, *Nature* **2017**, *552*, 219.
[46] D. A. Lauffenburger, A. F. Horwitz, *Cell* **1996**, *84*, 359.
[47] A. J. Ridley, M. A. Schwartz, K. Burridge, R. A. Firtel, M. H. Ginsberg, G. Borisy, J. T. Parsons, A. R. Horwitz, *Science* **2003**, *302*, 1704.
[48] K. Adebowale, Z. Gong, J. C. Hou, K. M. Wisdom, D. Garbett, H. Lee, S. Nam, T. Meyer, D. J. Odde, V. B. Shenoy, O. Chaudhuri, *Nat. Mater.* **2021**, *20*, 1290.
[49] S. Nam, J. Lee, D. G. Brownfield, O. Chaudhuri, *Biophys. J.* **2016**, *111*, 2296.
[50] J. M. Grolman, P. Weinand, D. J. Mooney, *Proc. Natl. Acad. Sci. USA* **2020**, *117*, 25999.
[51] A. Bershadsky, A. Chausovsky, E. Becker, A. Lyubimova, B. Geiger, *Curr. Biol.* **1996**, *6*, 1279.